Crystal Structures of Unbound and Aminooxyacetate-Bound Escherichia coli γ-Aminobutyrate Aminotransferase †

ARTICLE *in* BIOCHEMISTRY · SEPTEMBER 2004

Impact Factor: 3.02 · DOI: 10.1021/bi049218e · Source: PubMed

Crystal Structures of Unbound and Aminooxyacetate-Bound *Escherichia coli* γ-Aminobutyrate Aminotransferase†

Wenshe Liu, Peter E. Peterson, Richard J. Carter, Xianzhi Zhou, James A. Langston, Andrew J. Fisher, and Michael D. Toney*

Department of Chemistry, University of California, Davis, California 95616

Received April 19, 2004; Revised Manuscript Received June 9, 2004

ABSTRACT: The X-ray crystal structures of *Escherichia coli* γ-aminobutyrate aminotransferase unbound and bound to the inhibitor aminooxyacetate are reported. The enzyme crystallizes from ammonium sulfate solutions in the $P3_221$ space group with a tetramer in the asymmetric unit. Diffraction data were collected to 2.4 Å resolution for the unliganded enzyme and 1.9 Å resolution for the aminooxyacetate complex. The overall structure of the enzyme is similar to those of other aminotransferase subgroup II enzymes. The ability of γ-aminobutyrate aminotransferase to act on primary amine substrates (γ-aminobutyrate) in the first half-reaction and α-amino acids in the second is proposed to be enabled by the presence of Glu211, whose side chain carboxylate alternates between interactions with Arg398 in the primary amine half-reaction and an alternative binding site in the α-amino acid half-reaction, in which Arg398 binds the substrate α-carboxylate. The specificity for a carboxylate group on the substrate side chain is due primarily to the presence of Arg141, but also requires substantial local main chain rearrangements relative to the structurally homologous enzyme dialkylglycine decarboxylase, which is specific for small alkyl side chains. No iron−sulfur cluster is found in the bacterial enzyme as was found in the pig enzyme [Storici, P., De Biase, D., Bossa, F., Bruno, S., Mozzarelli, A., Peneff, C., Silverman, R. B., and Schirmer, T. (2004) *J. Biol. Chem. 279*, 363−73.]. The binding of aminooxyacetate causes remarkably small changes in the active site structure, and no large domain movements are observed. Active site structure comparisons with pig γ-aminobutyrate aminotransferase and dialkylglycine decarboxylase are discussed.

γ-Aminobutyrate (GABA)[1] is the major inhibitory neurotransmitter in the mammalian brain (*1*). It has been suggested to be involved directly or indirectly in several neuropathologies and psychiatric disorders (*2*, *3*). It is produced by the pyridoxal 5′-phosphate-dependent enzyme glutamate decarboxylase (*4*). Degradation of GABA is achieved through a second PLP-dependent enzyme, γ-aminobutyrate aminotransferase, which is an established target for neuroactive drugs (*5*).

GABA-AT belongs to the aminotransferase subgroup II of PLP-dependent enzymes (*6*). Most of these enzymes operate by the same kinetic mechanism, consisting of two half-reactions in which the cofactor alternates between its aldehydic (PLP) and amino (PMP) forms. The GABA-AT catalyzed half-reactions are shown in Scheme 1. In the first half-reaction, GABA is converted to succinic semialdehyde and its γ-amino group is transferred to the cofactor to generate PMP. In the second half-reaction, α-ketoglutarate is converted to L-glutamate and the PLP form of the enzyme is regenerated.

The inhibition of GABA-AT alters the balance between its substrate GABA and its product L-glutamate, which is the major excitatory neurotransmitter in brain, resulting in the elevation of GABA concentration. This elevation of GABA concentration has been found to correlate with pharmacological and behavioral effects (*7*−*10*). Inhibition of GABA-AT by vinyl-GABA is currently used in the treatment of epilepsy. Another experimentally studied GABA elevating agent is aminooxyacetate, which was first introduced by Wallach in 1961 (*11*). AOA is a potent inhibitor of GABA-AT, as well as many other PLP-dependent enzymes, both in vivo and in vitro. The strong inhibitory activity of AOA is attributable to the O-alkylhydroxylamine function, which forms an oxime with enzyme-bound PLP. The inhibition of GABA-AT by AOA after systematic administration is long-lasting and associated with a marked increase in brain GABA concentration (*11*−*13*).

Here, the structures of unliganded GABA-AT from *Escherichia coli* and its complex with AOA are presented. The bacterial enzyme shows strong sequence homology to the mammalian isozyme, and the X-ray structures presented here show the active sites to be virtually identical in structure. The great advantage of working with the bacterial enzyme is the very high level of expression of soluble enzyme in

† Supported by grant GM54779 to MDT from the National Institutes of Health. The SSRL Structural Molecular Biology Program is supported by the Department of Energy, Office of Biological and Environmental Research, and by the National Institutes of Health, National Center for Research Resources, Biomedical Technology Program, and the National Institute of General Medical Sciences. W.L. is supported by grant 2001-07 of the University of California System-wide Biotechnology Research Program.

* Corresponding author. E-mail: mdtoney@ucdavis.edu. Tel: (530) 754-5282. Fax: (530) 752-8995.

[1] Abbreviations: GABA, γ-aminobutyrate; GABA-AT, γ-aminobutyrate aminotransferase; PLP, pyridoxal 5′-phosphate; PMP, pyridoxamine 5′-phosphate; AOA, aminooxyacetate; SSDH, succinic semialdehyde dehydrogenase; DGD, dialkylglycine decarboxylase.

10.1021/bi049218e CCC: $27.50
Published on Web 08/04/2004

Scheme 1

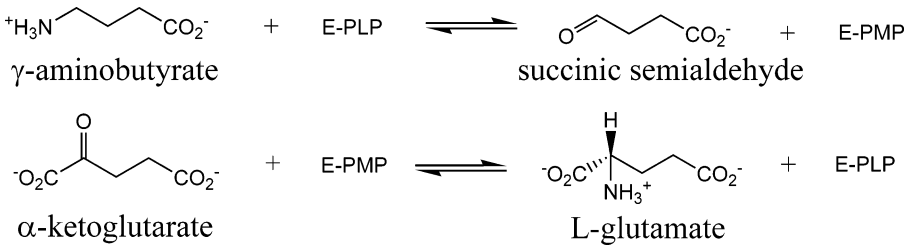

Escherichia coli, which enables the production of pure, readily crystallizable enzyme, and the characterization of active site mutants. Several active site mutants have been characterized. The kinetic properties of these, and the X-ray structures of three, will be presented in a separate publication.

EXPERIMENTAL PROCECURES

Materials. γ-Aminobutyric acid (GABA) was purchased from Aldrich. α-Ketoglutarate, pyridoxal 5′-phosphate, $NADP^+$, ADA, and aminooxyacetate (AOA) were from Sigma. Ammonium formate, ammonium sulfate, HEPES, and ethylene glycol were from Fisher.

Cloning, Expression, and Purification of Succinic Semialdehyde Dehydrogenase (SSDH). The *gabD* gene encoding $NADP^+$-dependent SSDH was obtained by PCR amplification of the gene from *E. coli* genomic DNA using Pfu DNA polymerase. The reverse primer contained a *BamHI* restriction site, while the forward primer contained an *NdeI* site. The amplified and digested SSDH gene was inserted into *NdeI*- and *BamHI*-digested pET23a (+) plasmid, which was transformed into *E. coli* BL21 (DE3). The transformants were grown at 37 °C in LB broth containing 50 μg/mL carbenicillin to $OD_{600} \approx 0.6$, induced with 0.5 mM IPTG, and then grown another 5 h at 37 °C. Cells were harvested by centrifugation for 15 min at 5000 rpm and resuspended in 20 mM ADA-KOH, pH 7.0, containing 10 mM DTT, 1 mM EDTA, 0.2 mg/mL lysozyme, and one tablet of protease inhibitors (Boehringer Mannheim). After stirring for 30 min at 4 °C, the cells were disrupted by sonication and the cell debris was removed by centrifugation at 15 000 rpm for 30 min. The supernatant from centrifugation was brought to 30% saturation in ammonium sulfate and equilibrated by stirring for 40 min at 4 °C. After centrifugation, the supernatant was brought to 65% saturation of ammonium sulfate, stirred for 40 min at 4 °C. The precipitate after 65% saturation of ammonium sulfate was redissolved in 20 mM ADA-KOH, pH 7.0, containing 10 mM DTT and 1 mM EDTA and dialyzed against the same buffer overnight. The sample was then applied to a 40 mL 2′,5′-ADP column (Pharmacia) and eluted with a 0 to 1 M linear gradient of KCl. The SSDH eluted at ~0.42 M KCl and was ~95% pure as indicated by SDS−PAGE. The protein concentration was assayed with the Bio-Rad DC assay, using IgG as standard. The enzyme activity was assayed using saturating succinic semialdehyde and $NADP^+$ (*14*).

Activity Assay of GABA-AT. The transamination reaction of GABA-AT with GABA and α-ketoglutarate was assayed by coupling the succinic semialdehyde produced to the reaction catalyzed by $NADP^+$-dependent SSDH. A Kontron UVIKON 9420 spectrometer was employed to monitor the increase in NADPH absorbance at 340 nm that occurs during the oxidation of succinate semialdehyde to succinate. Standard assay conditions were 30 mM TEA-HCl, pH 7.9, 100 μM PLP, 1 mM EDTA, 5 mM DTT, 3 unit/mL SSDH, 0.5 mM $NADP^+$, 10 mM GABA, and 2 mM α-ketoglutarate.

Cloning, Expression, and Purification of E. coli GABA-AT. The gene encoding GABA-AT was obtained by PCR amplification of the gene from *E. coli* genomic DNA using Pfu DNA polymerase, the right primer containing a *BamHI* restriction site and the left primer with an *NdeI* restriction site. The amplified and digested GABA-AT gene was inserted into *NdeI*- and *BamHI*-digested pET23a (+) plasmid. The recombinant plasmid was transformed into *E. coli* BL21 (DE3). The BL21 (DE3) transformants were grown at 37 °C in LB broth containing 50 μg/mL carbenicillin to $OD_{600} \approx 0.6$, induced with 0.5 mM IPTG, and then grown another 5 h at 37 °C. Cells were harvested by centrifugation for 15 min at 5000 rpm and resuspended in 16 mL of buffer A (20 mM TEA-HCl, pH 7.5, 100 μM PLP, 1 mM DTT, and 1 mM EDTA) containing 0.2 mg/mL lysozyme and one tablet of protease inhibitors (Boehringer Mannheim) at 4 °C. The mixture was stirred at 4 °C for 30 min. Cells were then disrupted by sonication and centrifuged at 15 000 rpm for 30 min to remove cell debris. The supernatant from centrifugation was brought to 30% saturation in ammonium sulfate and equilibrated by stirring for 40 min at 4 °C. After centrifugation, the supernatant was brought to 65% saturation of ammonium sulfate, stirred for 40 min at 4 °C, and the precipitate was dissolved in a large volume of buffer A until the conductivity of the protein solution was equivalent to that of buffer A containing 0.15 M KCl. The dissolved precipitate was loaded onto a 150 mL Q-sepharose Fast Flow (Pharmacia) and then eluted with a linear gradient of 0.15 M KCl to 0.45 M KCl in buffer A at a flow rate of 2 mL/min. Fractions were assayed for activity. GABA-AT was eluted at approximately 0.3 M KCl. The active fractions were pooled and GABA-AT was precipitated with 65% saturated ammonium sulfate. The precipitate was resuspended in buffer A and adjusted to the same conductivity as buffer A with 0.8 M ammonium sulfate. This solution was loaded onto a 70 mL high-performance Phenyl Sepharose (Pharmacia) column. The column was eluted with a linear 0.8 M to 0.5 M ammonium sulfate gradient in buffer A. GABA-AT was eluted at ~0.65 M ammonium sulfate. The active fractions were pooled, concentrated, and dialyzed against 10 mM potassium phosphate, pH 7.0, and 100 μM PLP. The enzyme was then applied to a 20 mL hydroxyapatite column (Bio-Rad) and eluted with a linear gradient of pH 7.0 potassium phosphate from 10 mM to 200 mM, with 100 μM PLP. GABA-AT was eluted at ~70 mM potassium phosphate. The active fractions were pooled together and concentrated. Homogeneous GABA-AT was demonstrated by a single band

Table 1: Data Collection and Refinement Statistics

	native	AOA complex
unit cell dimensions		
$a = b$, c (Å)	108.09, 301.25	108.15, 301.48
space group	$P3_221$	$P3_221$
no. of monomers per asymmetric unit	4	4
resolution range (Å)	30.0−2.4	30.0−1.9
R_{sym}[a] (%)	7.5 (34.5)	4.3 (18.0)
$\langle I\rangle/\sigma\langle I\rangle$	9.1 (2.0)	15.4 (4.1)
no. of reflections	79 767	159 733
redundancy	3.4	4.3
completeness (%)	98.8 (95.2)	98.9 (94.0)
R_{factor}[b] (%)	16.5	15.9
R_{free}[c] (%)	21.1	18.6
no. of protein atoms	12 824	12 824
no. of cofactor atoms	60	84
no. of water molecules	1 036	1 208
no. of sulfate atoms	55	55
no. of ethylene glycol atoms	42	64
mean B-factor (Å^2)		
entire molecule	22.96	20.94
main chain	21.41	19.33
side chains	23.16	22.77
solvent	28.87	31.35
rmsd from ideality		
bond distances (Å)	0.009	0.016
bond angle (deg)	1.44	1.65

[a] $R_{sym} = \sum_j|I_j(hkl) - \langle I(hkl)\rangle|/\sum_j|I(hkl)|$, where I_j is the measured intensity of reflection j and $\langle I\rangle$ is the mean intensity over j reflections. Numbers in parentheses are for the highest resolution shell. [b] $R_{factor} = \sum||F_{obs}(hkl)| - |F_{calc}(hkl)||/\sum|F_{obs}(hkl)|$, where F_{obs} and F_{calc} are observed and calculated structure factors, respectively. No σ-cutoff was applied. [c] R_{free} is the R factor calculated with 5% of the data that were not used for refinement.

on SDS−PAGE even when the protein was overloaded. Protein concentration was assayed with the Bio-Rad DC assay, using IgG as standard.

Crystallization and Data Collection for Native GABA-AT. The crystal screening of GABA-AT was performed using the hanging drop method. One μL of protein at a concentration of 20 mg/mL in 70 mM potassium phosphate, pH 7.0, and 100 μM PLP was mixed with an equal volume of reservoir solution containing different precipitants or salts in varying pH. Small crystals were found within 0.1 M HEPES−KOH, pH 7.6 or 7.8, and 1.6 M ammonium formate in the first round of screening. Refinement of the crystallization conditions was carried out. Large single crystals were obtained with 1.35 M ammonium sulfate instead of ammonium formate and 0.1 M HEPES−KOH, pH 7.6. Crystals generally appeared in a week and reached their maximal dimensions after three weeks. Crystals for data collection were cryoprotected using 30% ethylene glycol in the mother liquor for 1 or 2 h and immediately mounted in a loop and frozen in a nitrogen steam at 100 K. Data were collected on a Siemens HiStar multiwire dual detector using Cu Kα radiation, processed using SAINT (*15*), and scaled using ROTAVATA/AGROVATA from the CCP4 program suite (*16*). Crystal parameters and data collection statistics are given in Table 1.

Phasing. The program AMoRe was employed for molecular replacement, including self-rotation function calculations (*17*). A polyalanine model of GABA-AT was constructed from the structure of dialkylglycine decarboxylase (PDB code: 1DKA), which has 29% amino acid sequence identity and 53% similarity with GABA-AT. Data in the resolution range 30−4 Å were used in the molecular replacement. A dimeric search model produced a solution with a correlation coefficient of 50.3% and R-factor of 48.9%. The self-rotation search showed twofold noncrystallographic symmetry (NCS) in the asymmetric unit. Using the NCS, a mask was created using the program NCSMASK from the CCP4 program suite. This mask was used for density modification and phase extension from 4.0 Å to 2.6 Å using DM (*18*).

Model Building and Structure Refinement. The program O was used throughout for model building. Side chains were added to the polyalanine backbone of a monomer of GABA-AT and the tetramer was initially generated from noncrystallographic symmetry. The intermediate models were subjected to cycles of positional refinement, followed by simulated annealing, and B-factor refinement using CNS (*19*). Fo-Fc, 2Fo-Fc, and omit electron density maps were calculated at regular intervals to facilitate fitting. The refinement was monitored using the R_{free} calculated from 5% of the data. Once all the side chains had been modeled, the NCS constraints were removed and the four monomers were refined independently. Water molecules were added using CNS. The intermediate models were subjected to rigid body refinement, simulated annealing, and individual temperature factor refinement, and used for further density modification and phase extension. The sulfate ions and ethylene glycol molecules were inserted in the last round of refinement. Since ethylene glycol molecules without hydrogens have no rigid group required for torsion angle dynamics, those molecules were fixed in simulated annealing and their structure was refined only in the energy minimization steps. During refinement, two alternate conformations for S112 in chains A and D were found. They were generated using alternative conformation generation in CNS, and refined by fixing their occupancy at 0.5 and omitting interactions between them. The final refinement statistics are listed in Table 1.

Data Collection and Structure Refinement of GABA-AT Complex with AOA. AOA was diffused into crystals by soaking them in a cryoprotecting solution containing 0.1 HEPES−KOH, pH 7.6, 1.35 M ammonium sulfate, 5 mM AOA, and 30% ethylene glycol. The crystals were immediately mounted in a loop and frozen in a nitrogen steam at 100 K. Data were collected at 100 K using synchrotron beamline 9−2 at the Stanford Synchrotron Radiation Laboratory using a wavelength of 0.98 Å. Reflection intensities were integrated with DENZO and merged using SCALEPACK. The merged data were reduced to structure factors using the combination of SCALEPACK2MTZ, CAD, and TRUNCATE programs from the CCP4 program suite (*16*). The space group and unit cells parameters were unchanged from the native structure. Thus, the structure was solved using simulated annealing with the native GABA-AT structure (after deleting waters, ethylene glycols, sulfate ions, and PLP) as the starting model in CNS. In this initial step, refinements both with and without NCS restrictions were carried out. The R-factor obtained from refinement without the NCS restrictions was much lower than that obtained from refinement with them. Therefore, the structure after the refinement without NCS restriction was used to do cycles of positional, simulated annealing, energy minimization, and B-factor refinement from the CNS program suite and all four chains were refined individually without NCS restrictions. At the end of each round, difference Fourier and 2Fo-Fc electron-

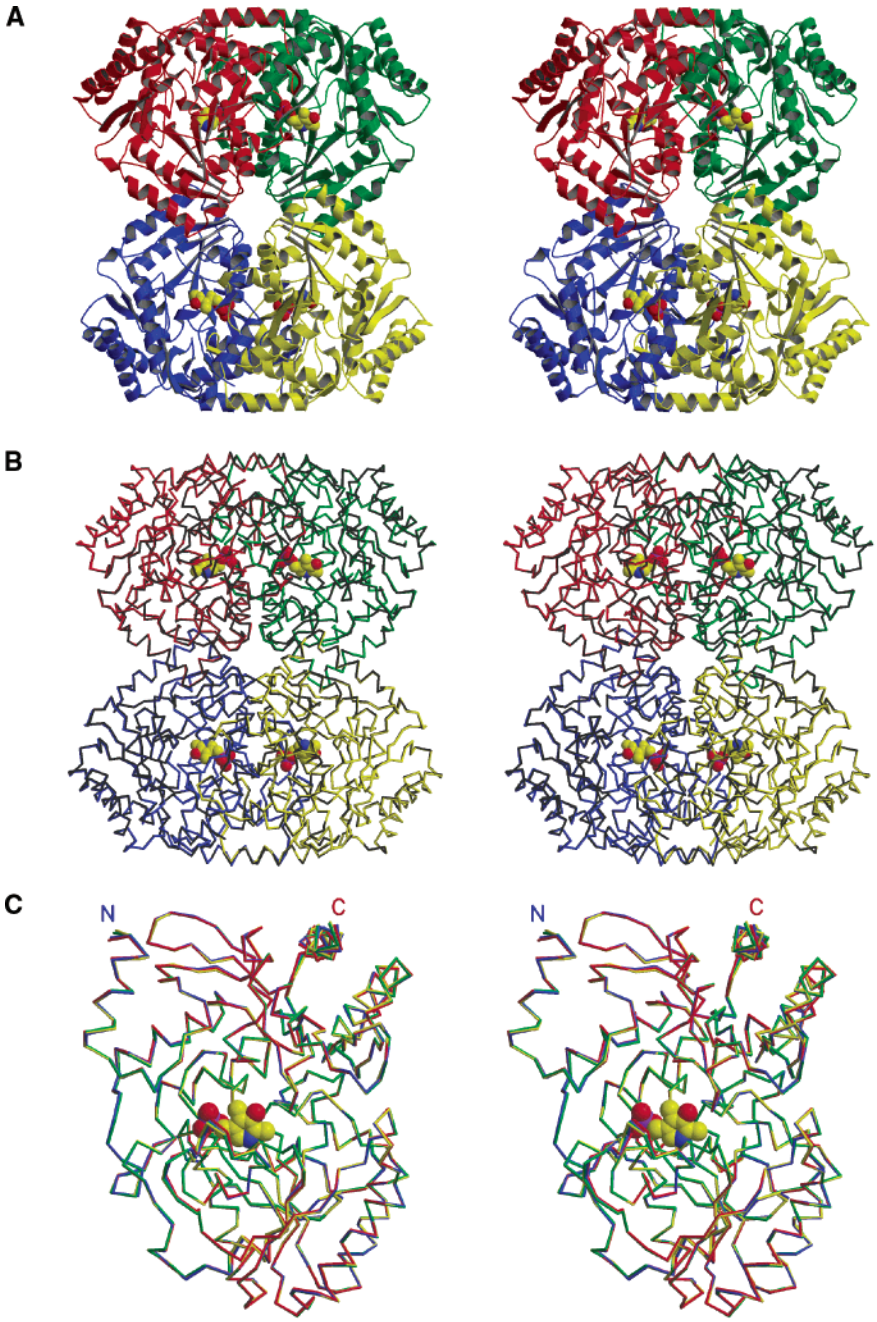

FIGURE 1: (A) Stereo cartoon representation of the native GABA-AT tetramer with the PLP cofactors shown as space-filling models. Red, monomer A; green, monomer B; blue, monomer C; and yellow, monomer D. (B) Superimposition of the Cα traces of native GABA-AT (colors as above) and GABA-AT complex with AOA (black). The r.m.s deviation between the Cα positions of these two structures is 0.22 Å. (C) The superimposition of the Cα traces of the four monomers (colors as above) in the asymmetric unit of native GABA-AT without AOA bound. The superimpositions presented here and in the following figures were obtained with SWISSPDB Viewer. The figures were made with MOLSCRIPT.

density maps were calculated. The program O was employed to correct and extend the model for phase extension by adding water molecules, ethylene glycol molecules, sulfate ions, and finally PLP-AOA. During refinement, two alternative conformations for both S112 and S217 were found in all four chains. They were generated and refined by fixing the occupancy for one conformer at 0.7 and the other at 0.3, since these occupancies gave the lowest R-factor. Crystal parameters, and data collection and refinement statistics are given in Table 1. The coordinates for native GABA-AT and its complex with AOA have been deposited in the Protein Data Bank (native GABA-AT, 1SF2; GABA-AT complex with AOA, 1SFF).

RESULTS

Overall Structure of Native GABA-AT. The biologically active structure of *E. coli* GABA-AT is an α_4-tetramer with 426 residues per subunit. Each of these four subunits was refined individually since the asymmetric unit contains a tetramer. The final refined structure has two residues with alternative conformations: Ser112 in monomers A and D. A schematic representation of the tetramer and Cα traces are presented in Figures 1A and 1B, while Figure 1C shows an overlay of the Cα traces of the four monomers in the asymmetric unit. Each of the four monomers in the asymmetric unit contains: (1) an N-terminal segment; (2) a large,

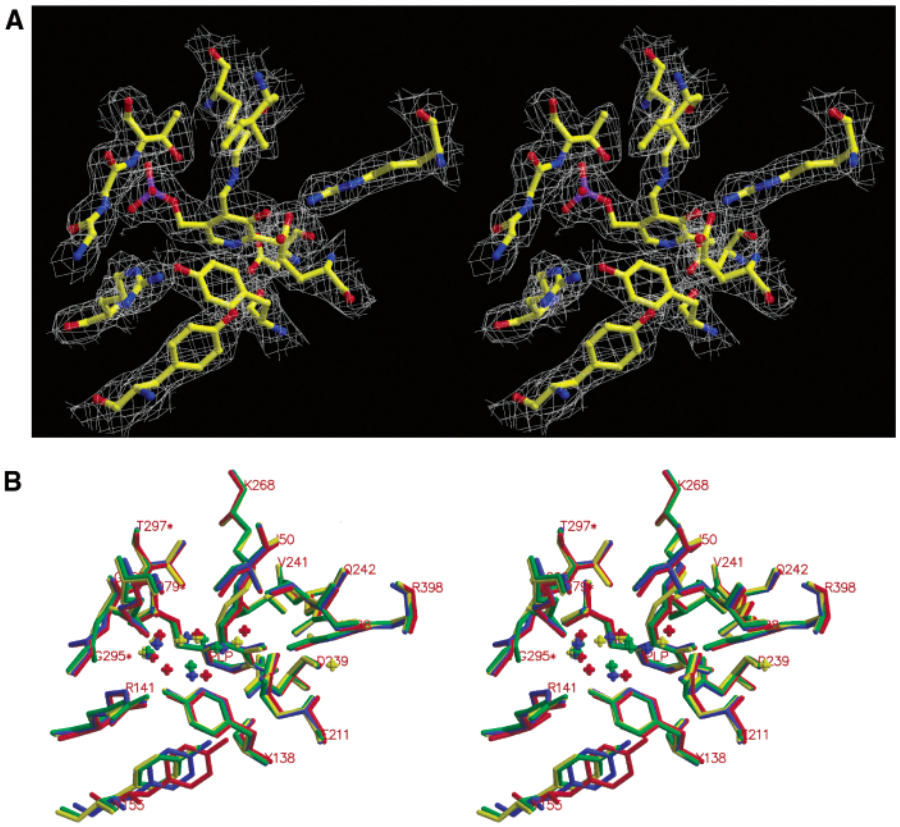

FIGURE 2: Stereo representation of the active site of native GABA-AT. (A) The 2Fo-Fc electron-density map for the active site residues and the cofactor. The map is contoured at 1.2σ. The figure was made with BOBSCRIPT. (B) Superimposition of four active sites (colors as in Figure 1A) in the asymmetric unit. Residues contributed from the second monomer are labeled with an asterisk (*).

PLP binding domain; and (3) a small, C-terminal domain. The N-terminal segment (residues 2 to 44) contains one α-helix and a three-stranded antiparallel β-sheet. The large domain (residues 49 to 321) comprises a central seven-stranded β-sheet surrounded by 11 α-helices. The C-terminal domain (residue from 323 to 426) is composed of three α-helices and a four-stranded antiparallel β-sheet, and is at the corners of the tetramer.

Superimposition of the four subunits in the asymmetric unit gives pairwise r.m.s deviations between 0.21 Å and 0.32 Å. The largest deviation is found in a loop region from residue 153 to 159. The largest displacement, which is between monomer A and monomer D, averages 1.23 Å. Other than this loop region there are no significant differences in structure between the four subunits in the asymmetric unit, even though they were refined individually.

Like DGD, two monomers make extensive contacts to form a dimer. The interaction surface between the two monomers is very large: 3620 Å^2 of solvent accessible surface, approximately one-quarter of the monomer surface, is buried on dimer formation. The two PLP cofactors are located close to the subunit interface of the dimer and close to each other (the PLP phosphorus atoms are 14.8 Å apart). Both active sites in the dimer are formed from residues contributed by both monomers. The tetramer is formed by the looser association of two dimers, lending approximate overall 222 noncrystallographic symmetry. The tetramer interface is much smaller than the dimer interface: only 340 Å^2 of solvent-accessible surface per monomer is buried on tetramer formation. Compared to DGD, which buries 1220 Å^2 of solvent-accessible surface per monomer during the tetramer formation, the dimer-dimer interaction in *E. coli* GABA-AT is weak. This was confirmed by gel filtration experiments, in which it was shown that a fraction of the enzyme exists as dimers (data not shown). Increasing the PLP concentration promotes tetramer formation.

Active Site Structure. Figure 2 presents the active site structure of *E. coli* GABA-AT. PLP is bound in a distinct cleft in the enzyme and is involved in many specific interactions. The C4′ atom, originally forming an aldehyde with oxygen, connects covalently to the ϵ-amino group of Lys268 forming the internal aldimine (Schiff base) linkage. This aldimine is believed to be protonated, since the nitrogen forms a hydrogen bond with the phenolic oxygen of PLP and is roughly in the plane of the pyridine ring (the torsion angle varies from 8° to 30° in the monomers). The absorbance spectrum of GABA-AT in solution shows a strong peak near 405 nm (data not shown), which is additional evidence for the protonated aldimine. In addition to the hydrogen bond made with the aldimine nitrogen, the 3′ phenolic oxygen of PLP makes a hydrogen bond with the side chain amide nitrogen of Gln242, and interacts with a water molecule that is additionally hydrogen bonded to the backbone nitrogen of Glu211 and the side chain carboxylate of Glu206. The pyridine nitrogen atom of PLP makes a salt bridge (2.80 Å) with Asp239. The pyridine ring is sandwiched between Tyr138 and Val241. The phenolic hydroxyl group of Tyr138 interacts with one of the nonester oxygens in the PLP phosphate via a water molecule. The phosphate group of PLP interacts with the N-terminus of an α-helix, which contributes Gly111 and Ser112 to the binding site. The phosphate group is held in the place by a total of nine

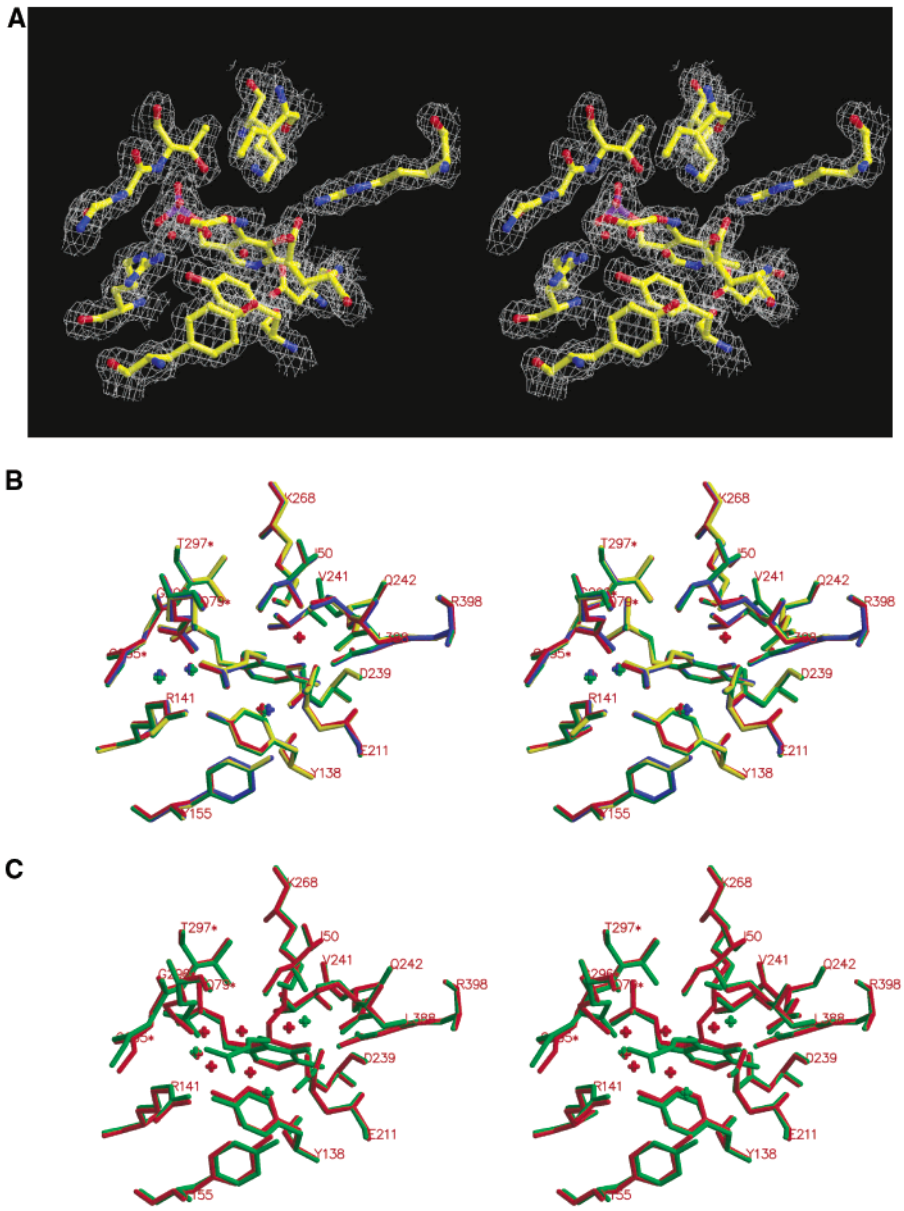

FIGURE 3: Stereo representation of the active sites of the GABA-AT complex with AOA. (A) The 2Fo-Fc electron-density map for the active site residues and the cofactor. The map is contoured at 1.2σ. The figure was made with BOBSCRIPT. (B) Superimposition of four active sites (colors as in Figure 1A) of GABA-AT complex with AOA. (C) Superimposition of the active sites of native GABA-AT (red) and GABA-AT complex with AOA (green).

hydrogen bonds to the nonester oxygens (saturating its hydrogen bonding capacity), four of which are donated by water molecules. Thr297* and Ser112 both donate a pair of hydrogen bonds from main chain nitrogen and side chain oxygen atoms. Figure 2 shows additional residues in the substrate-binding cleft and the potential roles of these will be discussed below. Figure 2B presents the superposition of the four active site structures of the tetramer. The structures of all four active sites are very similar except for Tyr155, which belongs to a loop region that shows the largest structural variation.

GABA-AT Complex with AOA. The structure of the GABA-AT complex with AOA was refined using unliganded GABA-AT as a model. Ser112 and Ser217 in all four monomers were found to have alternative conformations. Figure 3A presents the electron density map of GABA-AT obtained for GABA-AT crystals soaked in AOA. It clearly shows covalent modification of PLP at the active site. The Schiff base between PLP and the Lys268 ϵ-amino group has been broken. In its place, a Schiff base is formed between the amino group of AOA and PLP. The Schiff base nitrogen is roughly in the plane of the PLP pyridine ring (the torsion angle varying from 20° to 27°) and forms a hydrogen bond with the phenolic oxygen of PLP. The carboxylate group of AOA is held tightly in place by a salt bridge with Arg141 and a hydrogen bond with a water molecule. This water molecule makes two additional hydrogen bonds with the phenolic oxygen of Tyr155 and one carboxylate oxygen of Glu211. Figure 3B presents an overlay of the active site structures of the four monomers in the asymmetric unit. No significant differences in the active sites in the tetramer are observed. Figure 3C presents an overlay of the structures of both unliganded GABA-AT and its complex with AOA. The pyridine ring of the GABA-AT complex

with AOA is tilted compared to its orientation in the unliganded structure; the tilt angle increases by approximately 5°. Otherwise, the active site structures are remarkably similar, as are the Cα traces of the tetramer (Figure 1B; r.m.s deviation = 0.22 Å^2 for all Cα atoms). Thus, unlike aspartate aminotransferase, GABA-AT does not undergo domain closure on binding an inhibitor. Unlike the unliganded GABA-AT structure, Tyr155 does not show large deviations between the four subunits in the tetramer. The structure shows that AOA binding enlists a water molecule into the active site. This water molecule forms a hydrogen bond with Tyr155 making it less mobile.

Comparisons with Pig GABA-AT and DGD. The pairwise sequence identities for *E. coli* GABA-AT, pig GABA-AT, and DGD (the search model used for molecular replacement here) are 29% for *E. coli* GABA-AT vs pig GABA-AT, 29% for *E. coli* GABA-AT vs DGD, and 23% for pig GABA-AT vs DGD. Figures 4A and 4B present overlays of the Cα traces of these enzymes. Unlike *E. coli* GABA-AT, pig GABA-AT is an α_2-dimer, as are many PLP dependent enzymes. Nevertheless, the domain structure and overall fold are strongly conserved within all three enzymes. The Cα traces are remarkably similar with only small differences in loop regions. For example, there are significant differences in the loop region (residues 176−179 in the *E. coli* GABA-AT and residues 176−185 in DGD shown in the right side of Figure 4B) that forms the dimer-dimer interface in the *E. coli* GABA-AT and DGD tetramers, which is absent in pig GABA-AT. A superposition of *E. coli* GABA-AT and pig GABA-AT results in overall Cα r.m.s deviations of 1.27 Å at the monomer level and 1.46 Å at the dimer level for structurally homologous Cαs. The superposition of *E. coli* GABA-AT and DGD results in Cα r.m.s deviations of 1.21 Å at the monomer level, 1.25 Å at the dimer level, and 1.41 Å at the tetramer level for all corresponding Cα atoms. A unique feature of pig GABA-AT is the presence of an iron−sulfur cluster close to the PLP binding site (*20*), which is not found in *E. coli* GABA-AT or DGD.

Figure 4C presents an overlay of the active site structures of *E. coli* and pig GABA-ATs. There is complete conservation of residues that interact with PLP and nearly complete conservation of residues that interact with the substrates (or inhibitors as shown in Figure 4C). This is congruent with the fact that identical reactions are catalyzed by these enzymes. The strong active site conservation contrasts with the much lower overall sequence conservation.

An overlay of the active sites of *E. coli* GABA-AT and DGD is presented in Figure 4D. These active site structures differ significantly, as expected based on the different chemistry catalyzed by the enzymes. GABA-AT catalyzes transamination only, while DGD catalyzes both decarboxylation and transamination in its normal catalytic cycle. Additionally, the substrate specificities of these two enzymes differ, with *E. coli* GABA-AT accepting carboxylate-containing substrate side chains and DGD accepting only small alkyl substrate side chains. The decarboxylation specificity of DGD is thought to be largely determined by the presence of Gln52 in place of Ile50, while the carboxylate specificity of GABA-AT is thought to be due largely to the presence of Arg141 in place of Met141 in DGD. The implications of the active site structural differences to reaction and substrate specificity are discussed in more detail below.

DISCUSSION

The overall and active site structures of *E. coli* GABA-AT are quite similar to those of pig GABA-AT, DGD, and ornithine aminotransferase, while the overall fold is also similar to that of glutamate semialdehyde aminotransferase (*21*−*24*). It is interesting that *E. coli* GABA-AT does not have the iron−sulfur cluster that is present in pig GABA-AT near its active site (*20*). Clearly, it is not required for the basic chemistry catalyzed by the enzyme, but may perform a more complex regulatory role in the mammalian system. The folds of the monomers and the dimeric structures are highly conserved, while the higher order quaternary structures vary. For example, both *E. coli* GABA-AT and DGD are tetramers in solution (*22*), while pig GABA-AT is a dimer (*21*) and ornithine aminotransferase is a hexamer (*23*). The tetrameric and hexameric structures are simply higher order structures of the dimeric structure, which is obligatory since the active site is composed of residues from both subunits in the dimer. Ligand-bound structures for DGD (*25*, *26*), pig GABA-AT (*20*), glutamate semialdehyde aminotransferase (*24*), ornithine amintransferase (*27*, *28*), and now *E. coli* GABA-AT are available. None of these structures shows large-scale conformational changes compared to the unliganded structures, and it now appears that one can draw the general conclusion that the aminotransferase subgroup II enzymes do not undergo domain closure upon ligand binding, as do subgroup I enzymes (*29*).

The active site structure of unliganded *E. coli* GABA-AT presented in Figure 2 shows several highly conserved residues. Lys268 forms a Schiff base with PLP in the resting enzyme and is strictly conserved in structurally homologous PLP-dependent enzyme structures. It provides for a facile transimination pathway to the obligatory external aldimine intermediate, rather than *de novo* formation of the Schiff base from PLP and the amine substrate (*22*). Once freed in the active site it can also function as a catalytic acid/base residue (*30*). Asp239 is also strictly conserved in structurally homologous enzymes. This residue is thought to enable the protonation of the pyridine nitrogen of PLP such that it is a strong electron sink for stabilizing carbanionic intermediates that occur in the reaction pathway. Arg398 is completely conserved in structurally homologous enzymes that act on α-amino acids. Its role is to form a hydrogen bond-salt bridge with the α-carboxylate of the substrates. Finally, Arg141 is conserved in structurally homologous enzymes that use dicarboxylic substrates, which includes all of those that employ α-ketoglutarate as the amino group acceptor.

GABA-AT, like ornithine aminotransferase, has a dual substrate specificity in the sense that it can transfer the amino group of both primary amines and α-amino acids. In one reversible half-reaction GABA is converted to succinate semialdehyde, while in the other reversible half-reaction α-ketoglutarate is converted to L-glutamate. Glu211 is juxtaposed to Arg398 and interacts strongly via a hydrogen bond-salt bridge with it in both the unliganded (Figure 2) and AOA-liganded (Figure 3) structures. Analogous glutamate residues are found in ornithine aminotransferase and pig GABA-AT, where they make similar interactions with the homologues of Arg398 (*20*, *21*, *23*, *28*). Unfortunately, no structures exist for these enzymes bound to substrates containing an α-carboxylate. It is thought that the role of

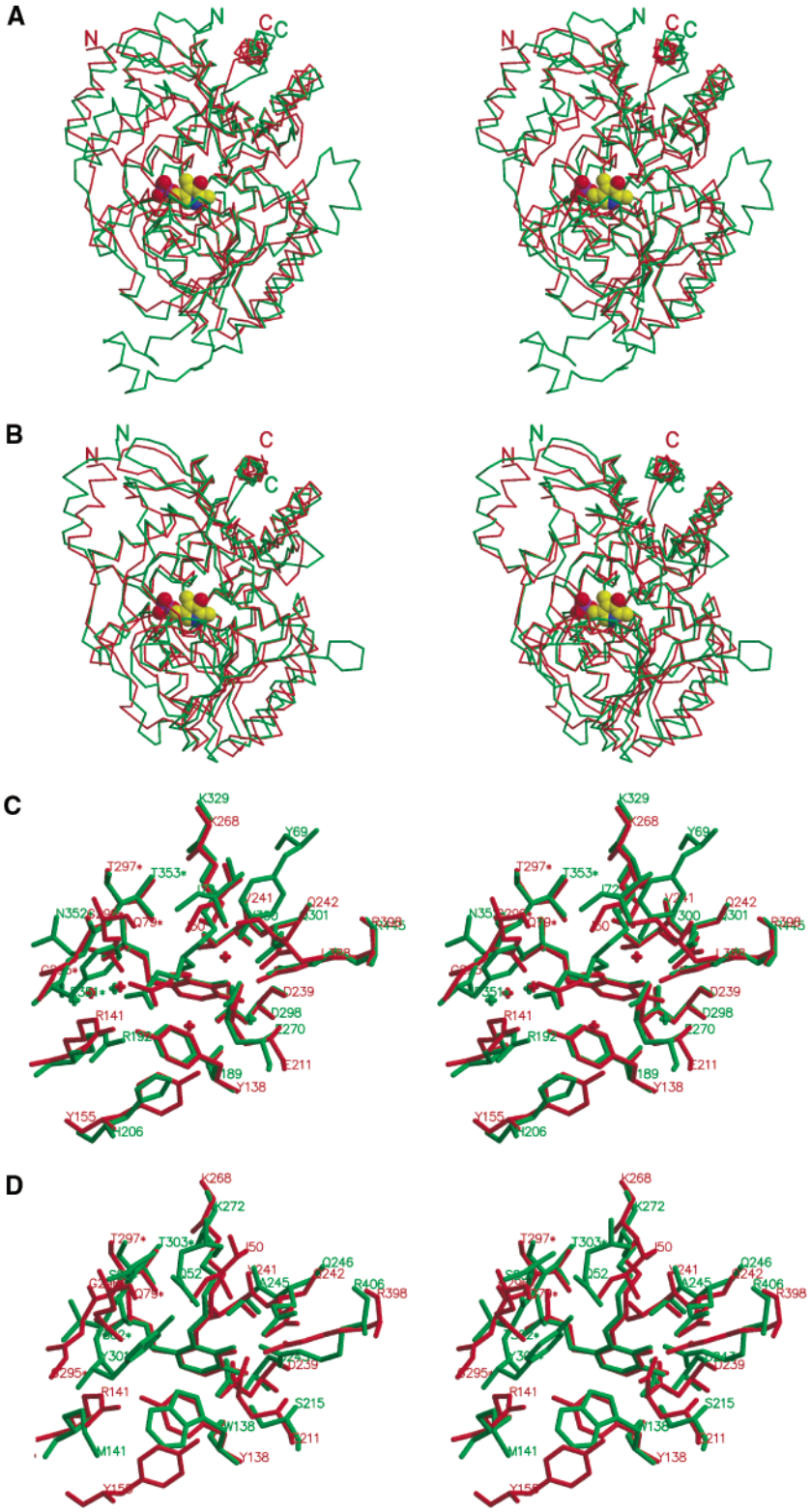

FIGURE 4: (A) Superimposition of the monomer Cα traces of *E. coli* GABA-AT (red) and pig GABA-AT (green). The N and C termini are marked. (B) Superimposition of the monomer Cα traces of *E. coli* GABA-AT (red) and DGD (green). (C) Superimposition of the active sites of native *E. coli* GABA-AT complexed with AOA (red) and pig GABA-AT complexed with γ-vinyl GABA (green). (D) Superimposition of the active sites of unbound *E. coli* GABA-AT (red) and DGD (green).

Glu211 is to neutralize the positive charge of Arg398 when primary amine substrates are bound at the active site. When α-amino acids are bound, it is expected that the Glu211 side chain rotates around the Cα-Cβ bond such that Arg398 is free to interact with the substrate carboxylate. Thus, the dual substrate specificity of GABA-AT, ornithine aminotransferase, and structurally homologous enzymes is likely the result of the ability of the enzyme to neutralize Arg398 via the Glu211 interaction when the substrate contains no carboxylate group. One might expect that an uncompensated positive charge near the reaction center would be detrimental to catalysis.

O-Alkylhydroxylamines such as AOA interact very strongly with aromatic aldehydes, and AOA is an inhibitor of many PLP dependent enzymes (*31*). The structure of the AOA complex shown in Figure 3 has, as expected, the terminal nitrogen of the inhibitor forming a Schiff base with PLP. This frees Lys268 to function as an acid/base catalyst in the proton transfers required for transamination. There are only very small changes in the active site structure in response to AOA binding, the largest being the ~5° change in tilt angle of the coenzyme and the freeing of Lys268.

AOA is an analogue of β-alanine (i.e., 3-aminopropionate), which is one methylene group shorter than GABA (4-aminobutyrate). The carboxylate oxygens of AOA make a side-on interaction with two nitrogens of the guanidino group of Arg141, which makes an additional hydrogen bond to the main chain carbonyl oxygen of Gly292 via the third nitrogen (not shown in Figure 3 for clarity). The AOA carboxylate oxygen-guanidino nitrogen interaction distances are rather long at 3.0 and 3.1 Å. It is likely that the longer structure of GABA will decrease these to more typical distances (2.7−2.9 Å), giving a stronger interaction with the carboxylate of the true substrate. The interaction of Arg141 with the main chain carbonyl of Gly292 appears to be important to localizing the Arg141 guanidino group in the correct location for optimal interaction with the carboxylate of GABA since this hydrogen bond (2.8 Å) does not lengthen in response to the shorter AOA side chain. This may be an important determinant of specificity for carboxylate groups on the γ-carbon of substrates.

The comparison between *E. coli* GABA-AT complexed with AOA and pig GABA-AT complexed with γ-vinyl GABA presented in Figure 4C shows remarkable conservation of the active site structures even though the overall identity between the enzymes is only 29%. This is undoubtedly dictated by the identity of the reactions catalyzed. Residues just outside of the substrate/coenzyme contacting shell, such as Gln79 and Tyr155, do show substitutions between the isozymes. These structural results suggest that employing the readily available *E. coli* enzyme in place of the difficult-to-obtain pig or human enzymes for mechanistic and/or inhibitor design studies is reasonable.

Figure 4D shows an overlay of the active site of *E. coli* GABA-AT and DGD. GABA-AT catalyzes only transamination half-reactions, while DGD catalyzes the oxidative decarboxylation of 2,2-dialkylglycines in its first half-reaction followed by transamination (a reductive amination) of pyruvate in the second half-reaction (*22*). It was previously proposed that Gln52 is important to the decarboxylation half-reaction of DGD by providing a substrate carboxylate binding site that activates this group stereoelectronically for decarboxylation (*22*, *25*). Interestingly, the structurally homologous residue in GABA-AT is a conserved isoleucine (Ile50), which is incapable of hydrogen bonding to a substrate α-carboxylate. The presence of Ser215 in DGD where Glu211 is located in GABA-AT is rationalized on the basis of the substrate specificity of DGD, which uses substrates containing α-carboxylate groups in both half-reactions. In GABA-AT, Glu211 interacts with Arg406 (in place of a substrate α-carboxylate) when primary amines are bound as substrate.

Finally, the side chain binding sites of *E. coli* GABA-AT and DGD are substantially different, in accord with the specificity of GABA-AT for carboxylate-containing side chains and the specificity of DGD for small alkyl side chains (e.g., methyl and ethyl groups) (*32*, *33*). The two changes most obviously important to the specificity of GABA-AT for carboxylate-containing side chains are the mutation of Met141 in DGD to Arg141 in GABA-AT, and the mutation of Trp138 in DGD to Tyr138 in GABA-AT. The former provides charge/hydrogen-bonding interactions with the substrate carboxylate, while the latter reduces steric bulk to allow the carboxylate-containing side chain to interact with Arg141. In addition to these two differences between the enzymes, the stretch of polypeptide from Pro291−Gly296 in GABA-AT and the structurally homologous residues in DGD (Gly297−Thr302) differ substantially in their Cα traces. That for GABA-AT is moved away from the substrate binding site, relative to DGD, creating more space for the substrate side-chain interaction with Arg141. If GABA-AT were to have the structure of DGD in this region, it is apparent from Figure 4D that the substrate carboxylate could not interact with Arg141 due to the location of the main chain carbonyl of Tyr301 in DGD. Additionally, the apparently important hydrogen bond between Arg141 and the Gly292 carbonyl would not be present to position the guanidino group. Thus, the difference in side chain specificity between GABA-AT and DGD apparently originates from more than simply providing the potential for a hydrogen bonding/salt bridge interaction for substrates carboxylates with Arg141. The active site structure must undergo more substantial alterations to provide space for the larger substrate side chain and hydrogen bonding interactions to the Arg141 guanidino group, the primary determinant of charge specificity.

ACKNOWLEDGMENT

Portions of this research were carried out at the Stanford Synchrotron Radiation Laboratory, a national user facility operated by Stanford University on behalf of the U.S. Department of Energy, Office of Basic Energy Sciences.

REFERENCES

1. Schwartz, J. H. (1991) *Principles of Neural Science*, Prentice Hall International, Norwalk.
2. Lloyd, K. G. (1986) GABAergic theory of epilepsy, *Rev. Prat. 36*, 243−54.
3. Lloyd, K. G., Morselli, P. L., and Bartholini, G. (1987) GABA and affective disorders, *Med. Biol. 65*, 159−65.
4. Wong, C. G., Bottiglieri, T., and Snead, O. C., 3rd. (2003) GABA, gamma-hydroxybutyric acid, and neurological disease, *Ann. Neurol. 54 Suppl. 6*, S3−12.
5. Sarup, A., Larsson, O. M., and Schousboe, A. (2003) GABA transporters and GABA-transaminase as drug targets Curr Drug Target, *CNS Neurol. Disord. 2*, 269−77.
6. Mehta, P. K., Hale, T. I., and Christen, P. (1993) Aminotransferases: demonstration of homology and division into evolutionary subgroups, *Eur. J. Biochem. 214*, 549−61.
7. Iadarola, M. J., and Gale, K. (1981) Cellular compartments of GABA in brain and their relationship to anticonvulsant activity, *Mol. Cell. Biochem. 39*, 305−29.
8. Sherif, F. M. (1994) GABA-transaminase in brain and blood platelets: basic and clinical aspects, *Prog. Neuropsychopharmacol. Biol. Psychiatry 18*, 1219−33.
9. Sherif, F. M., and Ahmed, S. S. (1995) Basic aspects of GABA-transaminase in neuropsychiatric disorders, *Clin. Biochem. 28*, 145−54.
10. Sherif, F. M., Tawati, A. M., Ahmed, S. S., and Sharif, S. I. (1997) Basic aspects of GABA-transmission in alcoholism, with particular reference to GABA-transaminase, *Eur. Neuropsychopharmacol. 7*, 1−7.

11. Wallach, D. P. (1961) Studies on the GABA pathway. I. The inhibition of gamma-aminobutyric acid-alpha-ketoglutaric acid transaminase in vitro and in vivo by U-7524 (amino-oxyacetic acid), *Biochem. Pharmacol. 5*, 323−31.
12. Loscher, W., and Frey, H. H. (1978) Aminooxyacetic acid: correlation between biochemical effects, anticonvulsant action and toxicity in mice, *Biochem. Pharmacol. 27*, 103−8.
13. Kuriyama, K., Roberts, E., and Rubinstein, M. K. (1966) Elevation of gamma-aminobutyric acid in brain with amino-oxyacetic acid and susceptibility to convulsive seizures in mice: a quantitative reevaluation, *Biochem. Pharmacol. 15*, 221−36.
14. Bartsch, K., von Johnn-Marteville, A., and Schulz, A. (1990) Molecular analysis of two genes of the Escherichia coli gab cluster: nucleotide sequence of the glutamate: succinic semialdehyde transaminase gene (gabT) and characterization of the succinic semialdehyde dehydrogenase gene (gabD), *J. Bacteriol. 172*, 7035−42.
15. Bruker (1998), Bruker AXS Inc., Madison, Wisconsin, United States.
16. Collaborative Computational Project, N. (1994) The CCP4 suite: programs for protein crystallography, *Acta Crystallogr. D50*, 760−763.
17. Navaza, J. (2001) Implementation of molecular replacement in AMoRe *Acta Crystallogr., Sect. D 57*, 1367−72.
18. Cowtan, K. D., and Zhang, K. Y. (1999) Density modification for macromolecular phase improvement, *Prog. Biophys. Mol. Biol. 72*, 245−70.
19. Brunger, A. T., Adams, P. D., Clore, G. M., DeLano, W. L., Gros, P., Grosse-Kunstleve, R. W., Jiang, J. S., Kuszewski, J., Nilges, M., Pannu, N. S., Read, R. J., Rice, L. M., Simonson, T., and Warren, G. L. (1998) Crystallography & NMR system: A new software suite for macromolecular structure determination, *Acta Crystallogr., Sect. D 54* (Pt 5), 905−21.
20. Storici, P., De Biase, D., Bossa, F., Bruno, S., Mozzarelli, A., Peneff, C., Silverman, R. B., and Schirmer, T. (2004) Structures of gamma-aminobutyric acid (GABA) aminotransferase, a pyridoxal 5′-phosphate, and [2Fe-2S] cluster-containing enzyme, complexed with gamma-ethynyl-GABA and with the antiepilepsy drug vigabatrin, *J. Biol. Chem. 279*, 363−73.
21. Storici, P., Capitani, G., De Biase, D., Moser, M., John, R. A., Jansonius, J. N., and Schirmer, T. (1999) Crystal structure of GABA-aminotransferase, a target for antiepileptic drug therapy, *Biochemistry 38*, 8628−34.
22. Toney, M. D., Hohenester, E., Keller, J. W., and Jansonius, J. N. (1995) Structural and mechanistic analysis of two refined crystal structures of the pyridoxal phosphate-dependent enzyme dialkylglycine decarboxylase, *J. Mol. Biol. 245*, 151−79.
23. Shen, B. W., Hennig, M., Hohenester, E., Jansonius, J. N., and Schirmer, T. (1998) Crystal structure of human recombinant ornithine aminotransferase, *J. Mol. Biol. 277*, 81−102.
24. Hennig, M., Grimm, B., Contestabile, R., John, R. A., and Jansonius, J. N. (1997) Crystal structure of glutamate-1-semialdehyde aminomutase: an alpha2-dimeric vitamin B6-dependent enzyme with asymmetry in structure and active site reactivity, *Proc. Natl. Acad. Sci. U.S.A. 94*, 4866−71.
25. Malashkevich, V. N., Strop, P., Keller, J. W., Jansonius, J. N., and Toney, M. D. (1999) Crystal structures of dialkylglycine decarboxylase inhibitor complexes, *J. Mol. Biol. 294*, 193−200.
26. Liu, W., Rogers, C. J., Fisher, A. J., and Toney, M. D. (2002) Aminophosphonate inhibitors of dialkylglycine decarboxylase: structural basis for slow binding inhibition, *Biochemistry 41*, 12320−8.
27. Shah, S. A., Shen, B. W., and Brunger, A. T. (1997) Human ornithine aminotransferase complexed with L-canaline and gabaculine: structural basis for substrate recognition, *Structure 5*, 1067−75.
28. Storici, P., Capitani, G., Muller, R., Schirmer, T., and Jansonius, J. N. (1999) Crystal structure of human ornithine aminotransferase complexed with the highly specific and potent inhibitor 5-fluoromethylornithine, *J. Mol. Biol. 285*, 297−309.
29. John, R. A. (1995) Pyridoxal phosphate-dependent enzymes, *Biochem. Biophys. Acta 1248*, 81−96.
30. Toney, M. D., and Kirsch, J. F. (1993) Lysine 258 in aspartate aminotransferase: enforcer of the Circe effect for amino acid substrates and general-base catalyst for the 1,3-prototropic shift, *Biochemistry 32*, 1471−9.
31. John, R. A., and Charteris, A. (1978) The reaction of aminooxyacetate with pyridoxal phosphate-dependent enzymes, *Biochem. J. 171*, 771−9.
32. Sun, S., Zabinski, R. F., and Toney, M. D. (1998) Reactions of alternate substrates demonstrate stereoelectronic control of reactivity in dialkylglycine decarboxylase, *Biochemistry 37*, 3865−75.
33. Sun, S., Bagdassarian, C. K., and Toney, M. D. (1998) Pre-steady-state kinetic analysis of the reactions of alternate substrates with dialkylglycine decarboxylase, *Biochemistry 37*, 3876−85.

BI049218E